Supplementary Information

Structural and functional dissection of ASCT2 interaction with Syncytin-1 mediating cell-cell fusion

Anna M. Borowska, Krystof Stafl, Michal Sykora, Jan Rheinberger, Martin Travnicek, Lubomira Pecnova, Anna Janovska, Jiri Hejnar, Cristina Paulino, Dirk J. Slotboom, Katerina Trejbalova

Correspondence: DJS (d.j.slotboom@rug.nl) and KT (katerina.trejbalova@img.cas.cz)

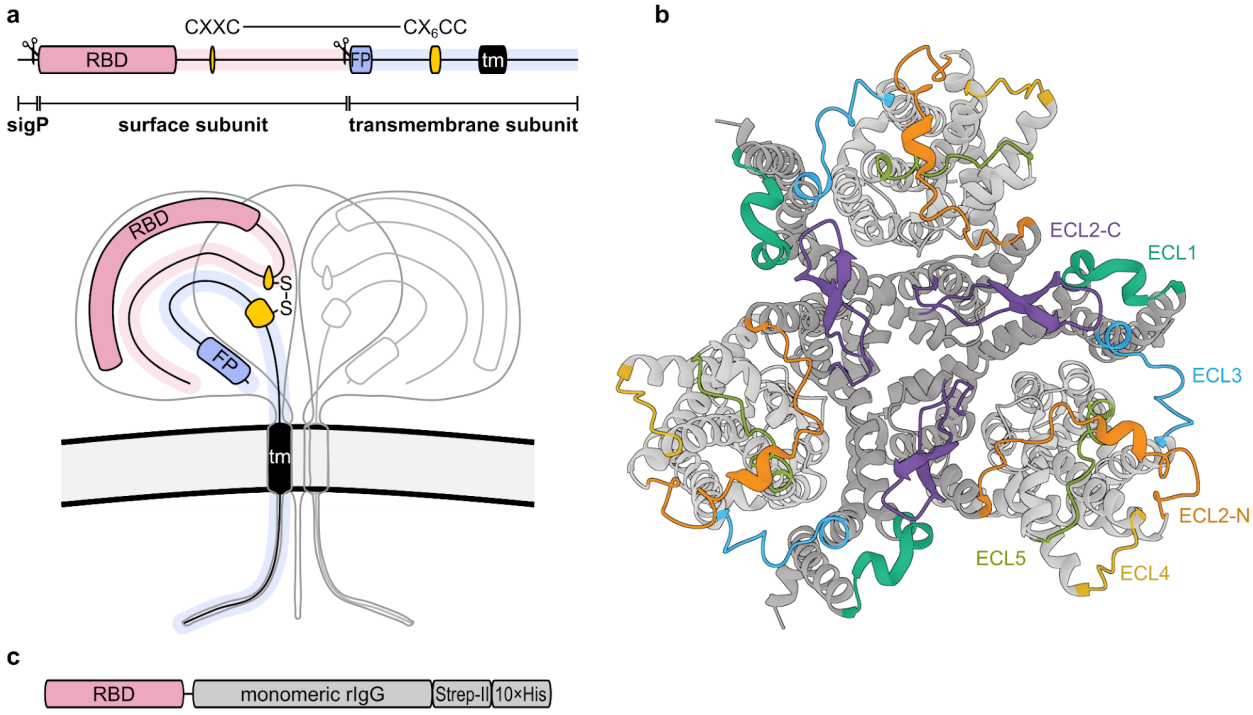

Supplementary Figure 1 – Structural architecture of Syncytin-1 and ASCT2. a, Organization of full-length Syncytin-1. The surface (SU) subunit is highlighted in pink and transmembrane (TM) subunit is shown in blue. Receptor-binding domain corresponds to residues 23 to 152 of the SU subunit and is highlighted in pink. The disulfide bond connecting the SU and TM subunits is colored as yellow, while the fusion peptide (FP) is in blue. Membrane boundaries are indicated by black lines with shadowed gray region. **b,** Cryo-EM structure of ASCT2 in the outward facing state (PDB 6MP6) showing the arrangement of the extracellular loops (ECL). The scaffold and transport domains are colored in dark and light gray, respectively. The extracellular loops are colored as follows: ECL1 in teal, C-terminus of ECL2 (ECL2-C) in purple, N-terminus of ECL2 (ECL2-N) in orange, ECL3 in blue, ECL4 in yellow, and ECL5 in olive green. **c,** Schematic representation of the S1-RBD construct used for complex formation. Syncytin-1 RBD is fused to the heavy chain of a monomeric rabbit IgG, followed by Strep-II and 10×His tags.

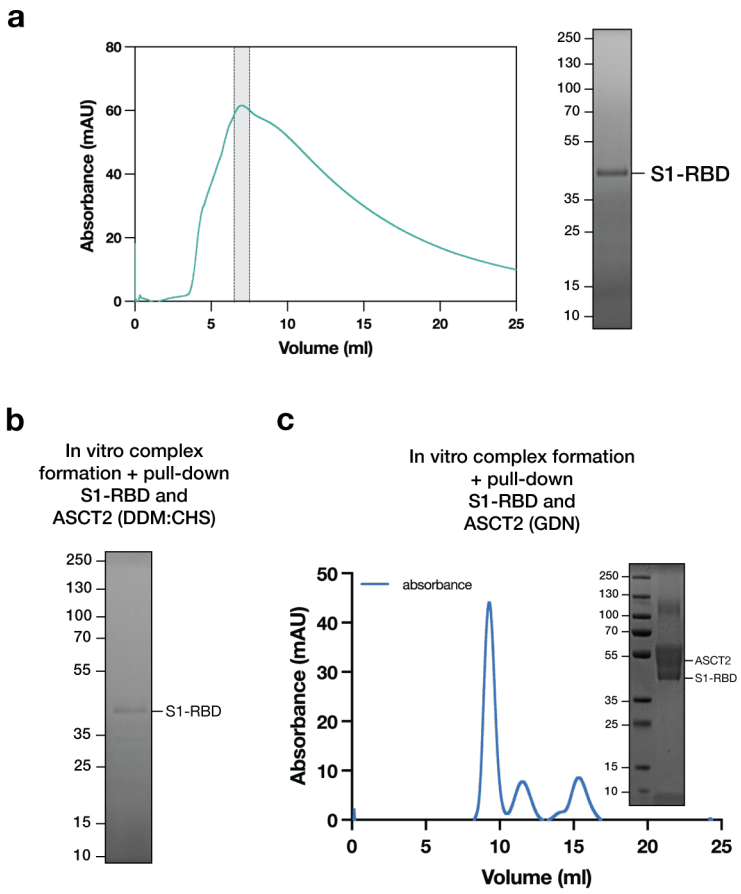

Supplementary Figure 2 – S1-RBD purification and ASCT2–S1-RBD complex formation. a, Elution profile of S1-RBD from the Strep-TactinXT affinity resin. The solid line represents the absorbance at 280 nm. The peak fraction is highlighted as gray area. SDS-PAGE gel analysis of the peak elution fraction highlighted in gray on the chromatogram. **b,** SDS-PAGE gel analysis showing lack of ASCT2-S1 complex formation via pull-down by S1-RBD with ASCT2 in DDM:CHS detergent, with only the purified S1-RBD found back after pull-down. **c,** Chromatogram of a SEC run of the ASCT2-S1-RBD complex formed by pulling down ASCT2 purified in GDN via S1-RBD. The inset shows SDS-PAGE gel analysis of the peak fraction. The solid line represents the absorbance at 280 nm.

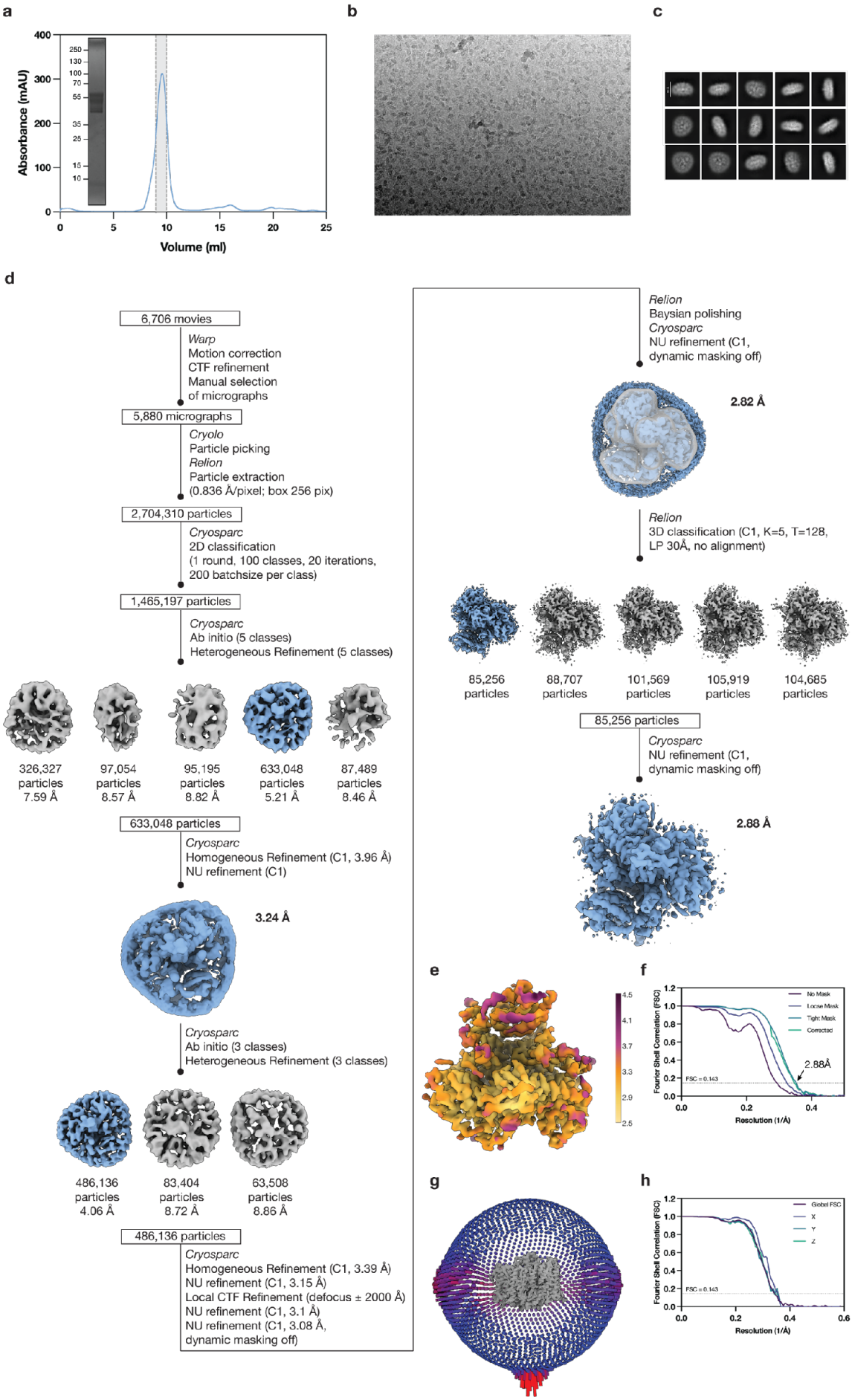
a
b
c
Absorbance (mAU)
Volume (ml)
d
6,706 movies
Warp
Motion correction
CTF refinement
Manual selection
of micrographs
5,880 micrographs
Cryolo
Particle picking
Relion
Particle extraction
(0.836 Å/pixel; box 256 pix)
2,704,310 particles
Cryosparc
2D classification
(1 round, 100 classes, 20 iterations,
200 batchsize per class)
1,465,197 particles
Cryosparc
Ab initio (5 classes)
Heterogeneous Refinement (5 classes)
326,327 particles 7.59 Å
97,054 particles 8.57 Å
95,195 particles 8.82 Å
633,048 particles 5.21 Å
87,489 particles 8.46 Å
633,048 particles
Cryosparc
Homogeneous Refinement (C1, 3.96 Å)
NU refinement (C1)
3.24 Å
Cryosparc
Ab initio (3 classes)
Heterogeneous Refinement (3 classes)
486,136 particles 4.06 Å
83,404 particles 8.72 Å
63,508 particles 8.86 Å
486,136 particles
Cryosparc
Homogeneous Refinement (C1, 3.39 Å)
NU refinement (C1, 3.15 Å)
Local CTF Refinement (defocus ± 2000 Å)
NU refinement (C1, 3.1 Å)
NU refinement (C1, 3.08 Å,
dynamic masking off)
Relion
Baysian polishing
Cryosparc
NU refinement (C1,
dynamic masking off)
2.82 Å
Relion
3D classification (C1, K=5, T=128,
LP 30Å, no alignment)
85,256 particles
88,707 particles
101,569 particles
105,919 particles
104,685 particles
85,256 particles
Cryosparc
NU refinement (C1,
dynamic masking off)
2.88 Å
e
f
Fourier Shell Correlation (FSC)
Resolution (1/Å)
No Mask
Loose Mask
Tight Mask
Corrected
2.88Å
FSC = 0.143
g
h
Global FSC
X
Y
Z

Supplementary Fig. 3 – Cryo-EM analysis of ASCT2 in complex with S1-RBD. a, SEC profile of ASCT2-S1-RBD complex with SDS-PAGE gel shown as inset. **b,** Representative cryo-EM image showing the ASCT2-S1-RBD particle distribution. **c,** Representative 2D class averages. **d,** Image processing workflow with final cryo-EM reconstructions (in blue) and mask used for postprocessing and 3D classification (transparent gray). Abbreviations: K = classes, T = tau. **e-h,** Validation of the ASCT2-S1-RBD. Shown are local resolution (**e**), Fourier shell correlation plot with indicated global resolution based on the threshold FSC = 0.143 (**f**), angular distribution (**g**), and anisotropy plot determined using the remote 3DFSC processing server (**h**).

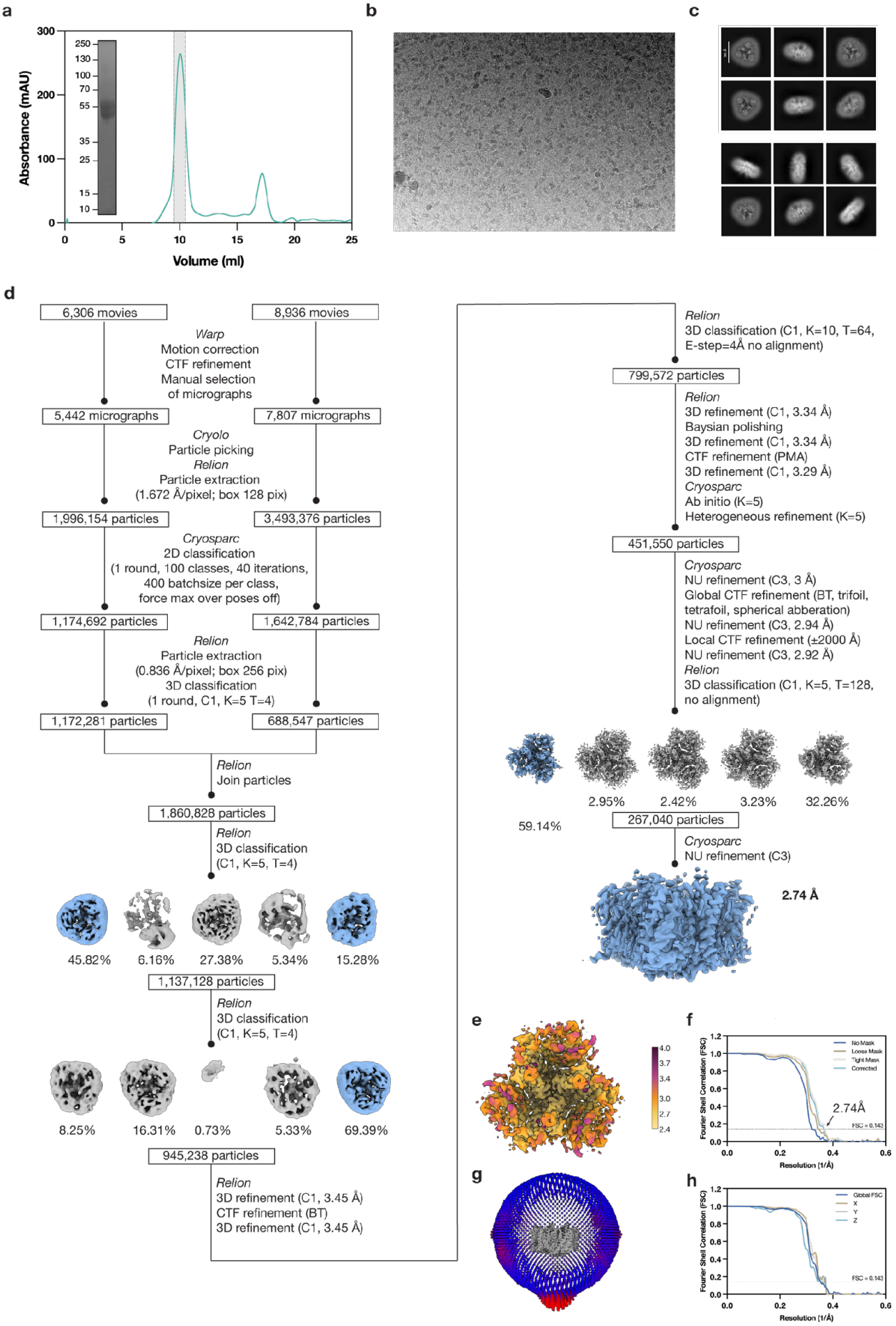
a
b
c
d
Absorbance (mAU)
Volume (ml)
6,306 movies
8,936 movies
Warp
Motion correction
CTF refinement
Manual selection
of micrographs
5,442 micrographs
7,807 micrographs
Cryolo
Particle picking
Relion
Particle extraction
(1.672 Å/pixel; box 128 pix)
1,996,154 particles
3,493,376 particles
Cryosparc
2D classification
(1 round, 100 classes, 40 iterations,
400 batchsize per class,
force max over poses off)
1,174,692 particles
1,642,784 particles
Relion
Particle extraction
(0.836 Å/pixel; box 256 pix)
3D classification
(1 round, C1, K=5 T=4)
1,172,281 particles
688,547 particles
Relion
Join particles
1,860,828 particles
Relion
3D classification
(C1, K=5, T=4)
45.82%
6.16%
27.38%
5.34%
15.28%
1,137,128 particles
Relion
3D classification
(C1, K=5, T=4)
8.25%
16.31%
0.73%
5.33%
69.39%
945,238 particles
Relion
3D refinement (C1, 3.45 Å)
CTF refinement (BT)
3D refinement (C1, 3.45 Å)
Relion
3D classification (C1, K=10, T=64,
E-step=4Å no alignment)
799,572 particles
Relion
3D refinement (C1, 3.34 Å)
Baysian polishing
3D refinement (C1, 3.34 Å)
CTF refinement (PMA)
3D refinement (C1, 3.29 Å)
Cryosparc
Ab initio (K=5)
Heterogeneous refinement (K=5)
451,550 particles
Cryosparc
NU refinement (C3, 3 Å)
Global CTF refinement (BT, trifoil,
tetrafoil, spherical abberation)
NU refinement (C3, 2.94 Å)
Local CTF refinement (±2000 Å)
NU refinement (C3, 2.92 Å)
Relion
3D classification (C1, K=5, T=128,
no alignment)
59.14%
2.95%
2.42%
3.23%
32.26%
267,040 particles
Cryosparc
NU refinement (C3)
2.74 Å
e
f
g
h
Fourier Shell Correlation (FSC)
Resolution (1/Å)
No Mask
Loose Mask
Tight Mask
Corrected
2.74Å
FSC = 0.143
Global FSC
X
Y
Z

Supplementary Figure 4 – Cryo-EM analysis of ASCT2 in GDN detergent. a, SEC profile of ASCT2 in GDN with SDS-PAGE gel shown as inset. **b,** Representative cryo-EM image showing the ASCT2 particle distribution. **c,** Representative 2D class averages. **d,** Image processing workflow with final cryo-EM reconstructions (in blue) and mask used for postprocessing and 3D classification (transparent gray). Abbreviations: K = classes, T = tau. **e-h,** Validation of the ASCT2 cryo-EM map. Shown are local resolution (**e**), Fourier shell correlation plot with indicated global resolution based on the threshold FSC = 0.143 (**f**), angular distribution (**g**), and anisotropy plot determined using the remote 3DFSC processing server (**h**).

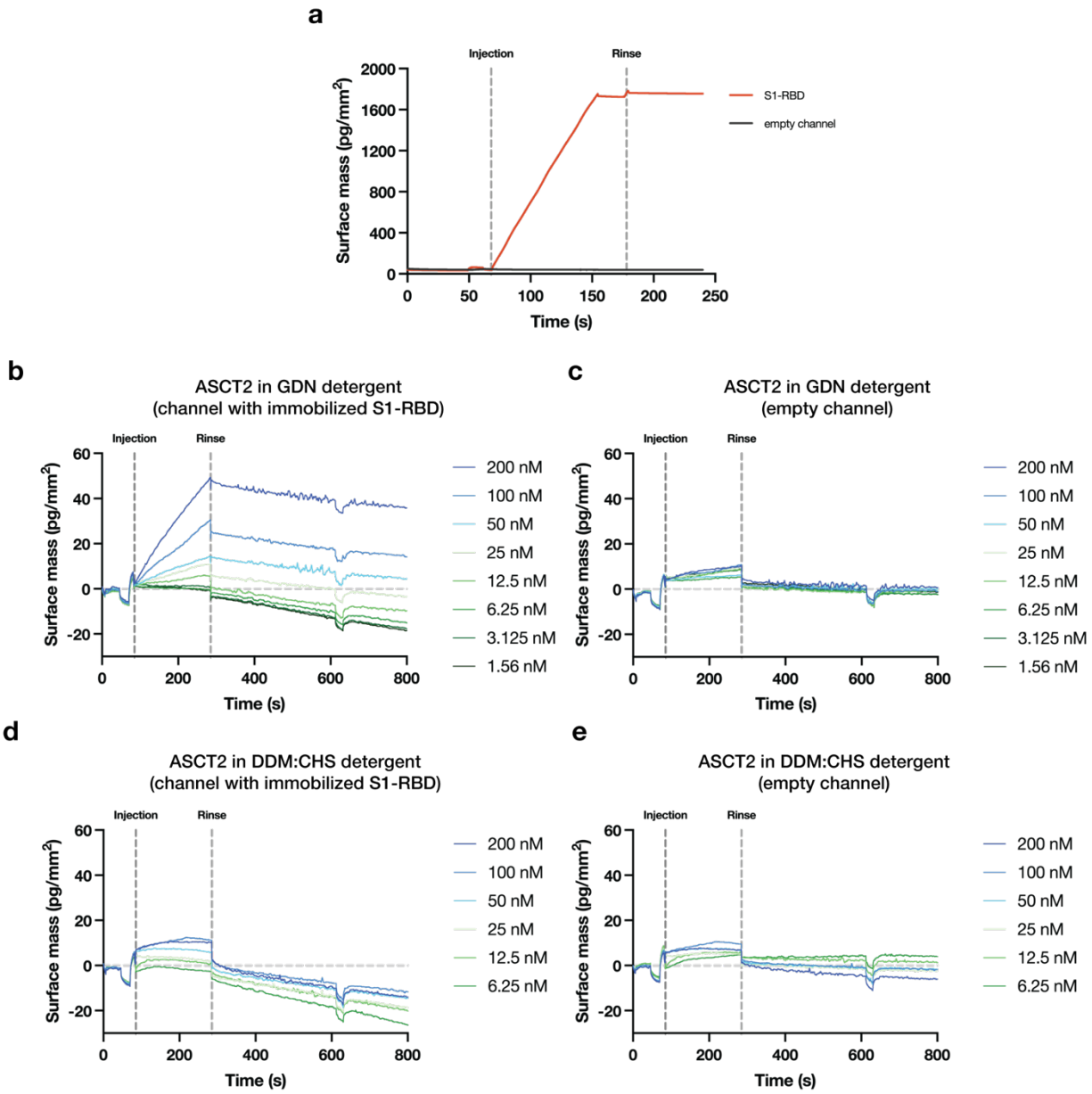

Supplementary Fig. 5 – GCI analysis of ASCT2 binding to S1-RBD. a, Representative sensogram showing S1-RBD immobilization on a Protein G surface (red) with reference channel baseline (gray). Injection and rise points indicate the start of sample addition and buffer wash. **b-c,** Raw GCI signals for ASCT2 (GDN) injections at different concentrations to S1-RBD surface (**b**) and reference channel (**c**). **e-f,** Raw GCI signals for ASCT2 (DDM:CHS) injections at different concentrations to S1-RBD surface (**e**) and reference channel (**f**).

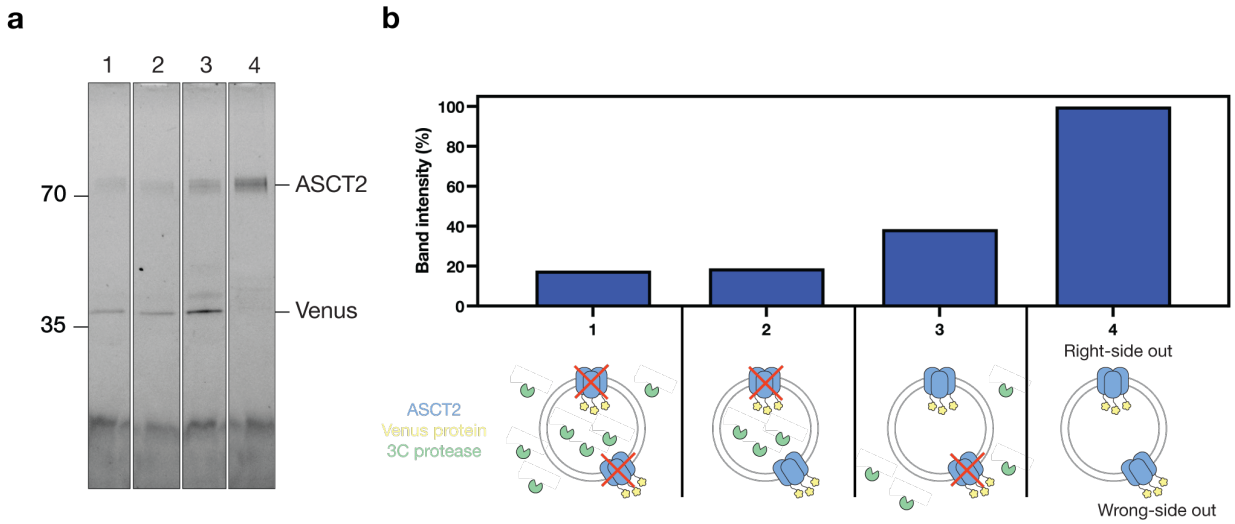

Supplementary Fig. 6 – ASCT2 orientation in liposomes. a, SDS-PAGE gel analysis of Venus-tagged ASCT2 reconstituted in liposomes, visualized by in-gel fluorescence of the Venus tag, under the following conditions: (1) liposomes loaded with the excess of 3C protease incubated with external 3C protease; (2) liposomes loaded with the excess of 3C protease incubated without any externally added 3C protease; (3) liposomes incubated with the excess of 3C protease; (4) liposomes not treated with 3C protease. **b,** Quantification of band intensities from (**a**) with a schematic of each condition. ASCT2 is shown in blue with Venus in yellow, and 3C protease in green. Band intensities were quantified in ImageJ.

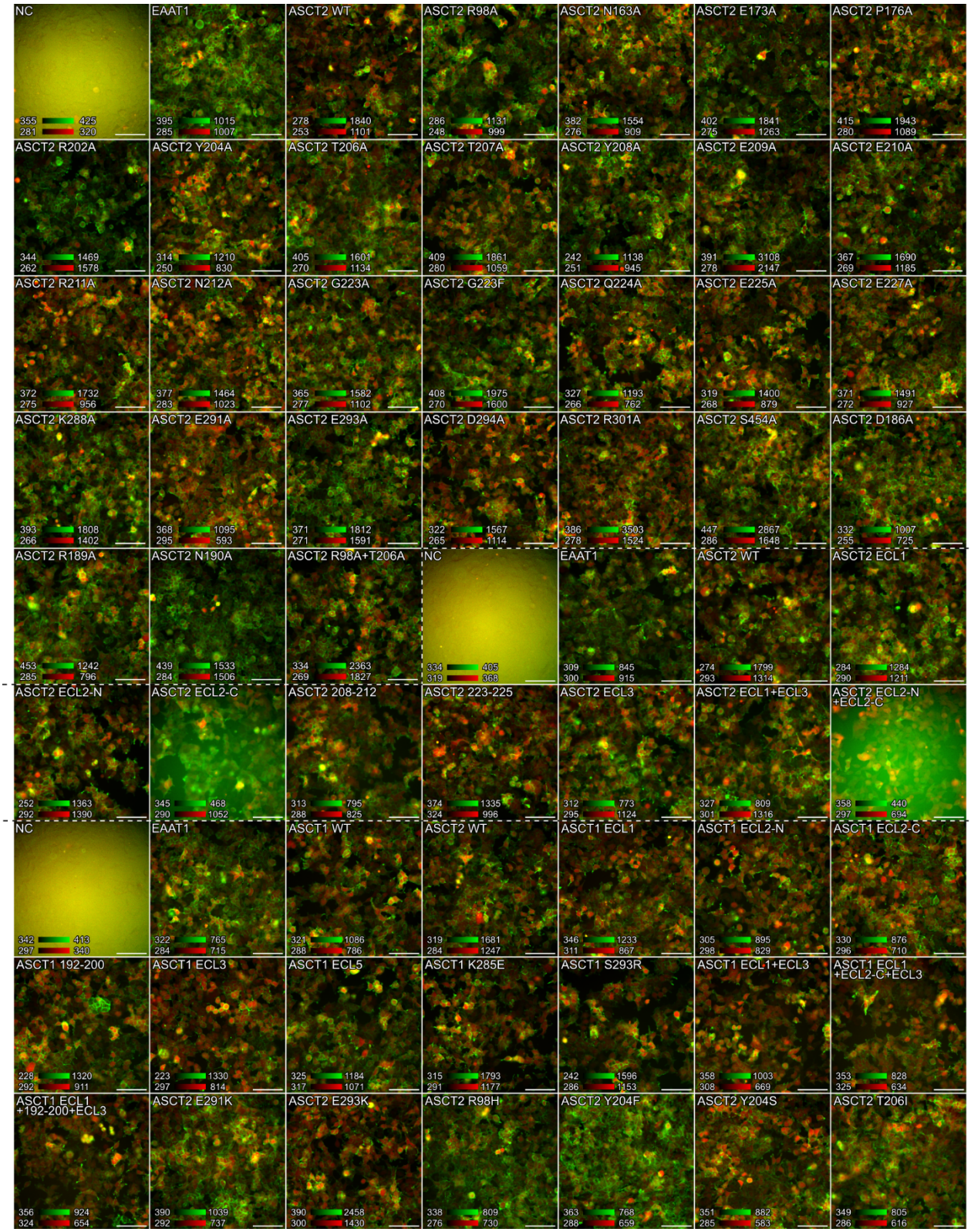

Supplementary Fig. 7 – Localization pattern of individual ASCT2 and ASCT1 mutants. Monochromatic 12-bit fluorescent images in green and infrared channels were captured with Nikon Ti2 microscope equipped with Nikon DS10 camera and 20× objective. Contrast was adjusted in ImageJ to values shown in the bottom left corners, images were converted to 8-bit, colorized and merged. Green channel shows localization of GFP-tagged transporter variants; red channel shows transduced cells expressing IRES-driven iRFP from transporter mRNA. White scale bars correspond to 100 μm. Dashed lines separate individual experiments.

NC, ASCT2/ASCT1 double-knockout HEK293T cells; EAAT1, double-knockout cells expressing EAAT1; WT, double-knockout cells expressing either wild-type ASCT1 or wild-type ASCT2.

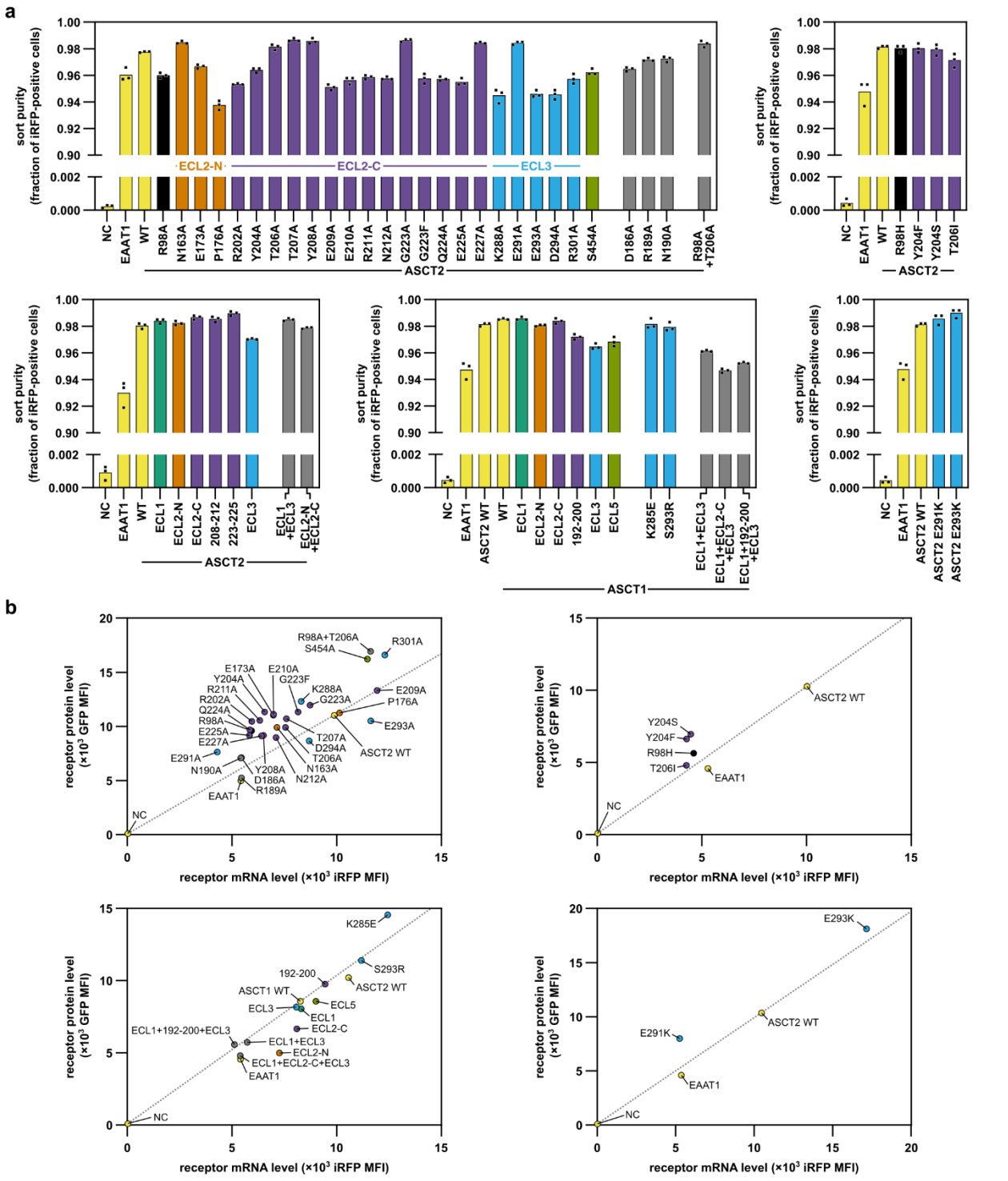

Supplementary Fig. 8 – Quality control of transduced transporter variants. a, Population purity of transduced cells represented by fraction of iRFP-expressing cells. Individual values of three independent measurements are shown with bars representing their means. **b,** Expression efficiency of receptor mutants, showing mRNA (x-axis) versus protein levels (y-axis). Average values of three independent measurements are shown. Dotted lines connecting NC and ASCT2 WT or ASCT1 WT show expected ratio of protein and mRNA levels. NC, ASCT2/ASCT1 double-knockout HEK293T cells; EAAT1, double-knockout cells expressing EAAT1; WT, double-knockout cells expressing either wild-type ASCT1 or wild-type ASCT2.

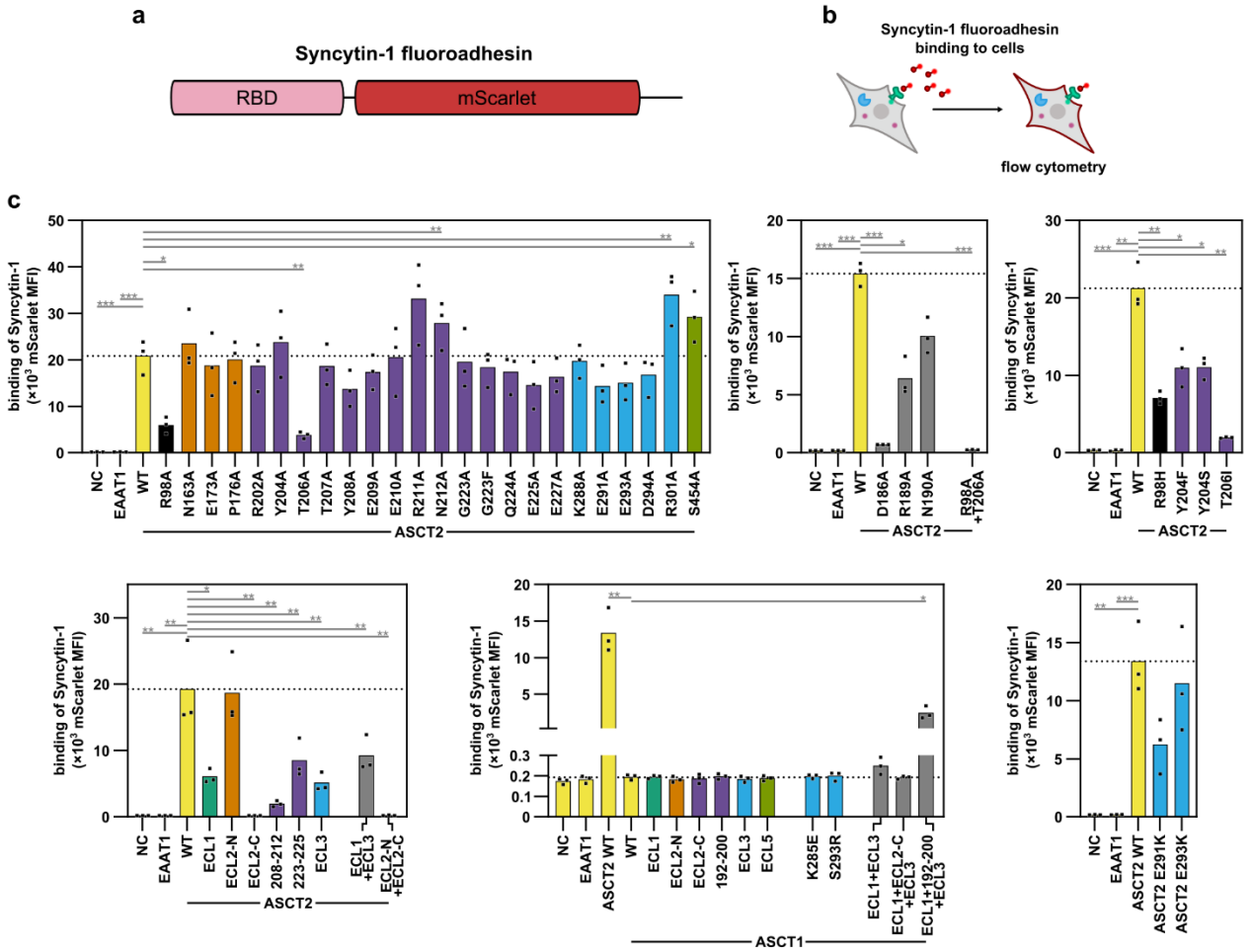

Supplementary Fig. 9 – Binding of S1-RBD fluoroadhesin to living cells expressing receptor variants. **a,** Schematic depiction of S1-RBD fluoroadhesin protein. **b,** Binding assay used for measurements. Cells expressing ASCT1 or ASCT2 variants were incubated with S1-RBD fluoroadhesin. Amounts of bound fluoroadhesin were detected by flow cytometry. **c,** Bound fluoroadhesin labeled cells with mScarlet and individual values of median fluorescent intensity (MFI) in three independent experiments are shown together with bars representing their means. Repeated-measures one-way ANOVA with Dunnett's post hoc test versus ASCT2 WT or ASCT1 WT was performed on log-transformed data and P-values are shown as follows: ∗, P<0.05; ∗∗, P<0.01; ∗∗∗, P<0.001. P-values higher than 0.05 are not shown. NC, ASCT2/ASCT1 double-knockout HEK293T cells; EAAT1, double-knockout cells expressing EAAT1; WT, double-knockout cells expressing either wild-type ASCT1 or wild-type ASCT2.

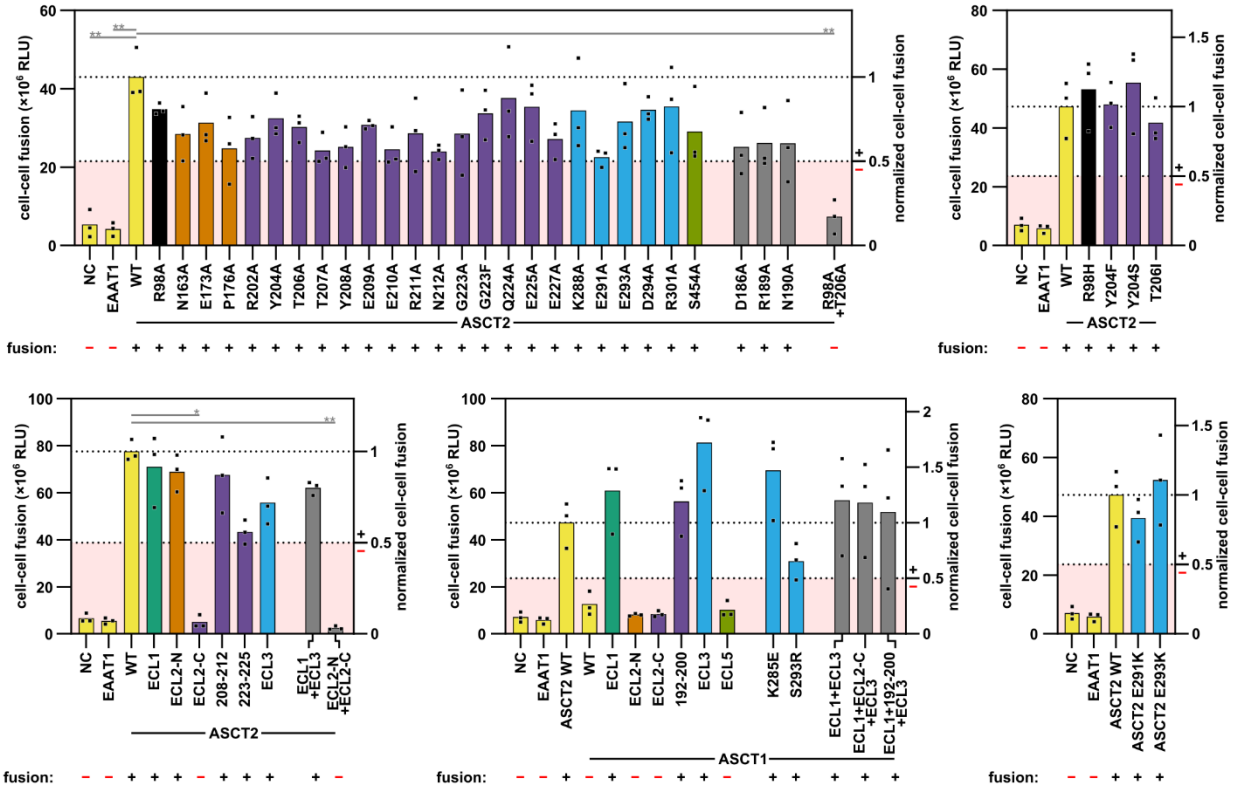

Supplementary Fig. 10 – Cell-cell fusion assay based on luciferase complementation. Relative luciferase units (RLU) from three independent experiments are shown, with bars indicating their means. Because the fusion event is inherently non-linear, the data were evaluated binarily. An arbitrary threshold was set at 50% of the signal observed in ASCT2 WT cells (bottom dotted line). Mutants with values above the threshold were classified as fusing (+), whereas those below the threshold were classified as non-fusing (−). As the data were not normally distributed, statistical significance was assessed using the Friedman test followed by Dunn's multiple comparisons test versus ASCT2 WT or ASCT1 WT. P-values are indicated as follows: ∗, $P < 0.05$; ∗∗, $P < 0.01$. P-values > 0.05 are not shown. NC, ASCT2/ASCT1 double-knockout HEK293T cells; EAAT1, double-knockout cells expressing EAAT1; WT, double-knockout cells expressing either wild-type ASCT1 or wild-type ASCT2.

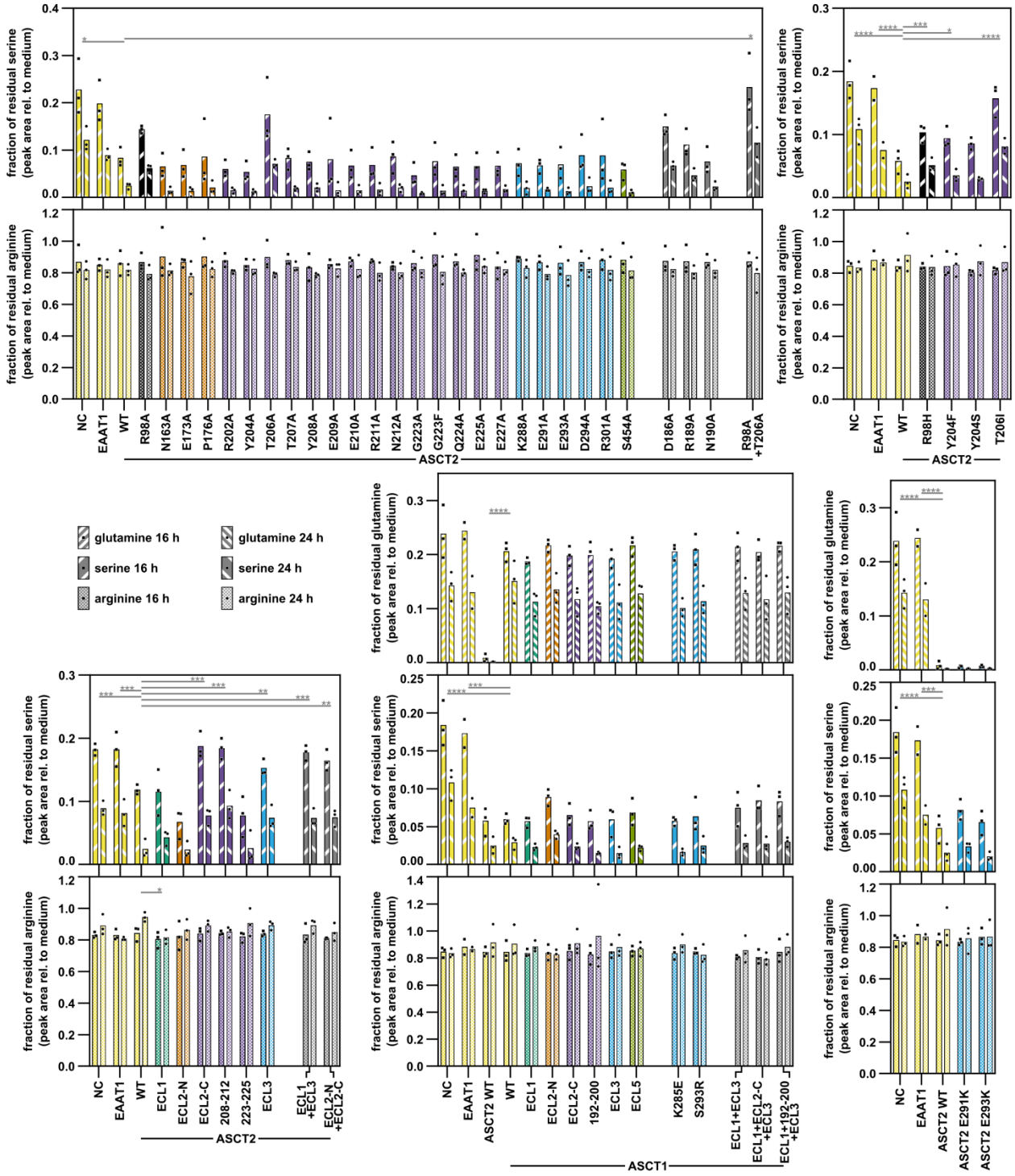

Supplementary Fig. 11 – Glutamine, serine, and arginine uptake by cells expressing individual receptor mutants. The uptake of deuterated amino acids is shown as fraction of their residual amount in the culture medium after 16 h or 24 h cultivation. Arginine was used as an internal standard as it is not transported by any of tested transporters. Values of three independent experiments are shown together with bars representing their means. Repeated-measures two-way ANOVA with Dunnett's post hoc test versus ASCT2 WT or ASCT1 WT was performed on log-transformed data and P-values are shown as follows: ∗, P<0.05; ∗∗, P<0.01; ∗∗∗, P<0.001; ∗∗∗∗, P<0.0001. P-values higher than 0.05 are not shown. NC, ASCT2/ASCT1 double-knockout HEK293T cells; EAAT1, double-knockout cells expressing EAAT1; WT, double-knockout cells expressing either wild-type ASCT1 or wild-type ASCT2.

Supplementary Fig. 12 – Sequence alignment of ASCT1 and ASCT2. The alignment was generated using MAFFT and ECL regions are highlighted.

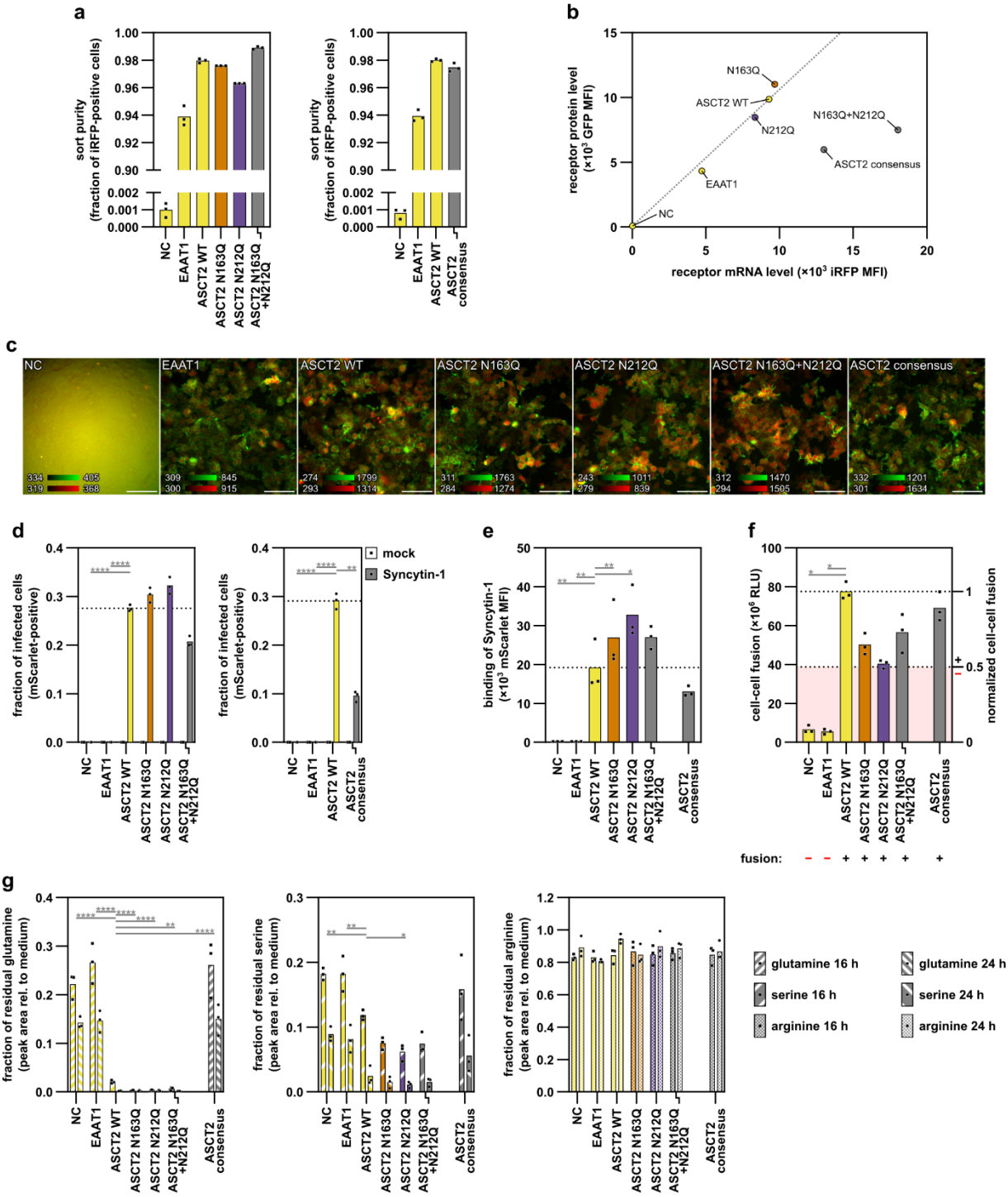

Supplementary Fig. 13 – Cells expressing deglycosylated and consensus variants of ASCT2 and their interaction with Syncytin-1. a, Population purity of transduced cells represented by fraction of iRFP-expressing cells. **b,** Expression analysis of ASCT2 extracellular loop mutants, comparing mRNA levels (median fluorescence intensity of iRFP, *x*-axis) and protein expression (median fluorescence intensity of GFP, *y*-axis). Average values of three independent measurements are shown. Dotted line connecting NC and ASCT2 WT shows expected ratio of protein and mRNA levels. **c,** Localization pattern of ASCT2 mutants. Monochromatic 12-bit fluorescent images in green and infrared channels were captured with Nikon Ti2 microscope equipped with Nikon DS10 camera and 20× objective. Contrast was adjusted in ImageJ to values shown in the bottom left corners, images were converted to 8-bit, colorized and merged. Green channel shows localization of GFP-tagged transporter variants; red channel shows transduced cells expressing IRES-

driven iRFP from transporter mRNA. White scale bars correspond to 100 μm. **d,** Infection efficiency of cells expressing individual ASCT2 mutants by Syncytin-1-pseudotyped virus. Repeated-measures two-way ANOVA with Dunnett's post hoc test versus ASCT2 WT was performed on data transformed with complementary log-log regression. **e,** Binding of S1-RBD fluoroadhesin to living cells expressing ASCT2 mutants. Bound fluoroadhesin labeled cells with mScarlet and individual values of median fluorescent intensity (MFI) are shown. Repeated-measures one-way ANOVA with Dunnett's post hoc test versus ASCT2 WT was performed on log-transformed data. **f,** Cell-cell fusion assay based on luciferase complementation. Relative luciferase units (RLU) from three independent experiments are shown. Mutants with values above 50% of ASCT2 WT were classified as fusing (+), whereas those below the threshold were classified as non-fusing (−). Friedman test followed by Dunn's multiple comparisons test versus ASCT2 WT was performed. **g,** Glutamine, serine, and arginine uptake by cells expressing individual receptor mutants. The uptake of deuterated amino acids is shown as fraction of their residual amount in the culture medium after 16 h or 24 h cultivation. Repeated-measures two-way ANOVA with Dunnett's post hoc test versus ASCT2 WT was performed on log-transformed data. P-values are shown as follows: $*$, $P<0.05$; $**$, $P<0.01$; $***$, $P<0.001$; $****$, $P<0.0001$. P-values higher than 0.05 are not shown. NC, ASCT2/ASCT1 double-knockout HEK293T cells; EAAT1, double-knockout cells expressing EAAT1; WT, double-knockout cells expressing wild-type ASCT2.

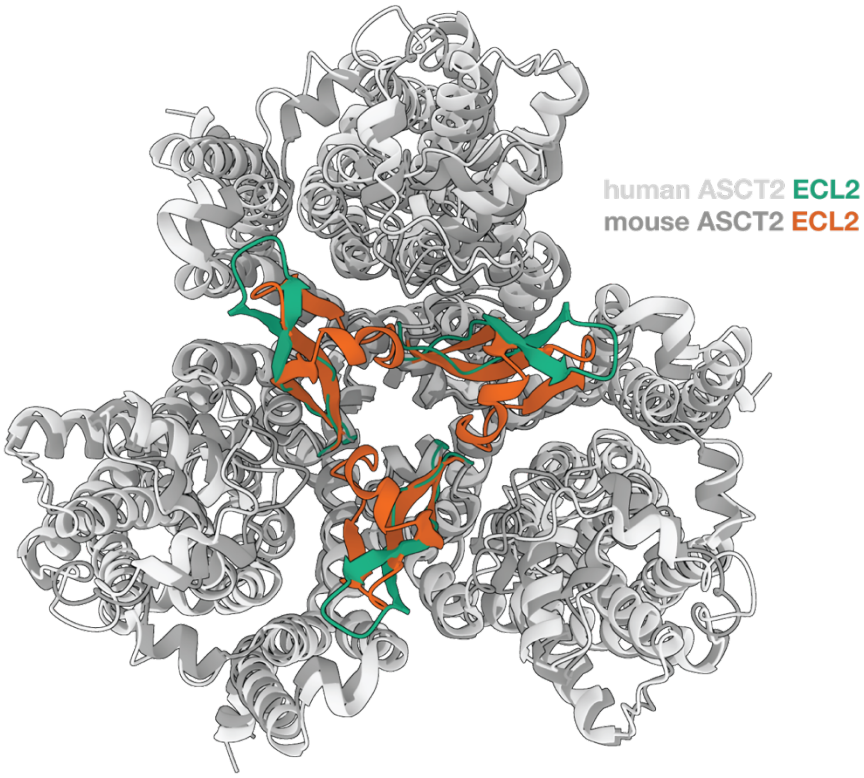

Supplementary Fig. 14 – Structural comparison of mouse and human ASCT2. Overlay of the mouse ASCT2 model predicted by AlphaFold3 (dark gray) and the human ASCT2 cryo-EM structure (light gray, PDB 6MP6), both shown in the outward-facing conformation. Extracellular loop 2 (ECL2) is highlighted to illustrate differences in length and positioning. ECL2 of human ASCT2 is shown in green, whereas ECL2 of mouse ASCT2 in orange.

Supplementary Table 1 – Cryo-EM data collection, refinement and validation statistics.

	ASCT2 in GDN (PDB ID 30LK, EMD-57883)	**ASCT2-S1-RBD complex in GDN (PDB ID 30LJ, EMD-57882)**
Data collection and processing		
Microscope	Thermo Fisher Titan Krios	
Detector	Gatan K3 Bioquantum	
Camera mode	Superresolution counting mode, binned by 2	
Voltage (kV)	300	
Nominal magnification	105,000	
Pixel size (Å)	0.836	
Number of frames	76	
Total electron exposure (e^{-}/Å^2)	59.9	60
Defocus range (μm)	-0.9 to -1.9	
Micrographs collected	15,242	6,706
Micrographs used	13,249	5,880
Total number of extracted particles	5,489,530	2,704,310
Final number of particles	267,040	1,465,197
Symmetry imposed	C3	C1
Global map resolution (Å) (FSC 0.143)	2.74	2.88
Map resolution range (Å)	~2.4 to 4.0	~2.5 to 4.0
Refinement		
Initial model used (PDB code)	8QRO	8QRO and 8OUJ
Model resolution (Å) (FSC 0.5)	2.9	3.2
Map sharpening	-120	
Model composition		
Chains	3	4
Non-hydrogen atoms	9450	10,749
Protein residues	1266	1441
Ligands		
Gln	3	3
R.m.s deviations		
Bond lengths (Å)	0.003	0.004
Bond angles (°)	0.582	0.603
Validation		
MolProbity score	1.26	1.37
Clashscore	4.94	6.47
Poor rotamers (%)	0.90	0.79
Ramachandran plot		
Favored (%)	98.31	97.97
Allowed (%)	1.69	2.03
Outliers (%)	0.00	0.00

Supplementary Table 2 – List of mutations introduced in ASCT2 constructs.

Construct name	Mutations
ECL1	deletion E84-RL-S87
ECL2-N	N163A, E173A, P176A
ECL2-C	Y204A, T206A, Y208A, E209A, E210A, R211A, N212A, G223A, Q224A, E225A
208-212	Y208A, E209A, E210A, R211A, N212A
223-225	G223A, Q224A, E225A
ECL3	K288A, E293A, D294A, R301A

Supplementary Table 3 – List of engineered ASCT1 variants featuring replaced extracellular loops with equivalent ASCT2 counterparts.

Loop	ASCT1		ASCT2	
	Number	Residues	Number	Residues
ECL1	68-74	S68-RTQVT-Y74	82-88	G82-PERLS-A88
ECL2-N	140-163	K140-PGSGAQTLQSSDLGLEDSGPPP-V163	154-175	Q154-PGAASAAINASVGAAGSAEN-A175
ECL2-C	190-218	T190-YATDYKVVTQNSSSGNVTHEKIPIGTE-I218	203-226	S203-YSTTYEERNITGTRVKVPVGQE-V226
192-200	192-200	A192-TDYKVVT-Q200	205-213	S205-TTYEERN-I213
ECL3	285-293	K285, V289, T292, S293	293-301	E293, L297, A300, R301
ECL5	446	P446	454	S454

Supplementary Table 4 – Comparison of receptor interfaces among enveloped viruses.

Family	Genus	PDB ID	Virus		Receptor		
			Name	Envelope glycoprotein	Name	Interacting residues within 3.5Å	Buried surface area (Å^2)
Retroviridae	Gammaretrovirus	this structure	HERV-W	Syncytin-1	ASCT2	37	3148.6
		8OUJ	HERV-W	Syncytin-1	ASCT2	31	3150.7
		8OUI	HERV-H	Suppressyn	ASCT2	28	2417
		7OIX	HERV-FRD	Syncytin-2	MFSD2A	13	1237.4
		9FQT	Friend murine leukemia virus (FrMLV)	Env	CAT1 (SLC7A1)	19	798.15
	Lentivirus	1GC1	Human immunodeficiency virus (HIV-1)	Env	CD4	17	1366.5
		3JCB	HIV-1	Env	CD4	15	1008.1
		6MEO	HIV-1	Env	CD4	14	1276.6
					CCR5	24	2034.1
Coronaviridae	Betacoronavirus	6M0J	Severe acute respiratory syndrome-related coronavirus (SARS-CoV-2)	Spike protein (S1)	ACE2	15	850.97
Filoviridae	Orthoebolavirus	5F1B	Zaire ebolavirus	Envelope glycoprotein (GP)	NPC1	11	808.15
		9DZ2	Sudan ebolavirus	Envelope glycoprotein (GP)	NPC1	11	707.09
Paramyxoviridae	Henipavirus	2VSM	Nipah virus	Nipah glycoprotein (G)	Ephrin-B2	23	2329
	Morbillivirus	3ALZ	Measles virus	Hemagglutinin glycoprotein (H)	SLAM	11	1002.3
		3INB	Measles virus	Hemagglutinin glycoprotein (H)	CD46	23	1092.2
		4GJT	Measles virus	Hemagglutinin glycoprotein (H)	HveC (Nectin-1)	15	1016.5
Arenaviridae	Mammarenavirus	3KAS	Machupo virus	Glycoprotein G1	TfR1	14	1087.2
Orthoherpesviridae	Simplexvirus	1JMA	Herpes simplex virus (HSV1)	Envelope glycoprotein D (gD)	HveA (TNR14)	14	822.44
		3SKU	HSV1	Envelope glycoprotein D (gD)	HveC (Nectin-1)	17	907.87
	Cytomegalovirus	7M22	Human cytomegalovirus	Envelope glycoproteins gH, gL, UL128, UL130, and UL131A	Neuropilin-2	4	710.86
	Rhadinovirus	7CZF	Kaposi Sarcoma associated herpesvirus (KSHV)	Envelope glycoproteins gH and gL	Ephrin-A2	13	1132.2

Supplementary Table 5 – MRM parameters for mass spectrometry analysis.

Compound ID	Q1 mass (Da)	Q3 mass (Da)	Dwell time (ms)	DP (V)	EP (V)	CE (V)	CXP (V)
L-Serine-d_3	109.1	63.1	28	35	10	16	8
L-Glutamine-d_5	152.1	88.0	28	50	10	25	8
L-Arginine-d_7	182.2	60.1	28	35	10	21	8